J. Appl. Comput. Mech., 8(1) (2022) 21-35
DOI: 10.22055/JACM.2019.14842

ISSN: 2383-4536
jacm.scu.ac.ir

Shahid Chamran University of Ahvaz

Journal of Applied and Computational Mechanics

Research Paper

Heat Transfer of Hybrid-nanofluids Flow Past a Permeable Flat Surface with Different Volume Fractions

N. Indumathi[1], B. Ganga[2], R. Jayaprakash[3], A.K. Abdul Hakeem[4]

[1] Department of Mathematics, Sri Ramakrishna Mission Vidyalaya College of Arts and Science, Coimbatore - 641 020, INDIA, Email: induramesh07@gmail.com

[2] Department of Mathematics, Providence College for Women, Coonoor - 643 104, INDIA, Email: gangabhose@gmail.com

[3] Department of Physics, Sri Ramakrishna Mission Vidyalaya College of Arts and Science, Coimbatore - 641 020, INDIA, Email: jayaprakash.rajan.2015@gmail.com

[4] Department of Mathematics, Sri Ramakrishna Mission Vidyalaya College of Arts and Science, Coimbatore - 641 020, INDIA, Email: abdulhakeem6@gmail.com

Received July 18 2019; Revised October 16 2019; Accepted for publication October 16 2019.
Corresponding author: A.K. Abdul Hakeem (abdulhakeem@rmv.ac.in, abdulhakeem6@gmail.com)

Abstract. Nowadays, the preparation, characterization, and modeling of nanofluids are deliberated in plenty to improve the heat transfer effects. Therefore, this paper centers on the heat transfer effects of three separate hybrid nanoparticles such as Al_2O_3-SiO_2, Al_2O_3-TiO_2, and TiO_2-SiO_2 with a base fluid such as water to gratify the advances. Analytical investigations for the Marangoni convection of different hybrid nanofluids over the flat surface for the cases such as suction, injection and impermeable were analyzed. A validation table for the comparison between analytical and numerical studies is tabulated. The influence of the hybrid nanoparticles solid volume fraction and the wall mass transfer parameter are mentioned through graphs at the side of the heat transfer rate tabulation. The impact of solid volume fraction decelerates the velocity distribution and raises the temperature distribution for all the three hybrid nanofluids in the cases of suction, impermeable, and injection. While relating the surface velocity and heat transfer rate of the three hybrid nanofluids, Al_2O_3-SiO_2/water has a higher surface velocity, TiO_2-SiO_2/water has a higher heat transfer rate and Al_2O_3-TiO_2/water has lower surface velocity and heat transfer rate for the increment of wall mass transfer parameter.

Keywords: Hybrid-nanofluids; Permeable surface; Marangoni convection; Laplace transform; Volume fraction.

1. Introduction

Two decades earlier, in order to improve the heat transfer properties of the fluid, nanoparticles are dispersed (1-100 nm) in the fluid. This fluid was first referred to as nanofluid by Choi [1] in 1995. Simultaneously, a variety of researches on the impacts of nanofluids on heat transfer were performed by the investigators experimentally and numerically. Nanofluids find application during a type of area like granular and fiber insulation, geothermal power and other energy sources extraction, drug delivery, industrial cooling applications, nuclear reactors, nanofluid detergent, etc.

Kulkarni et al. [2] have experimentally researched that the rise in the number of nanoparticles like CuO, Al_2O_3, and SiO_2 hikes the nanofluid heat transfer coefficient. Razali et al. [3] did a structural analysis and morphological study of Al_2O_3 nanofluids in a microchannel heat sink. Shen et al. [4] tested the important role of nanofluids on grinding cast iron which raises the surface roughness and reduces grinding forces due to the use of Al_2O_3/water and diamond/water nanofluid. Xuan et al. [5] experimentally discovered that the thermal conductivity of the Cu-H_2O nanofluid improved up

Published online: December 04 2019

to 5 percent. Further Abu Nada [6] reported that the metal with high thermal conductivity nanoparticles has possessed Nusselt number enhancement, as well as metal oxides nanoparticles with low thermal conductivity, also enhanced the heat transfer.

But these results are not gratified the engineering advancements. Combining two or more nanoparticles into a base fluid is known as hybrid nanofluid. The materials of these combined nanoparticles are selected appropriately, according to the positive aspects of each other. Applications of hybrid nanofluids are generator cooling, biomedical, solar energy conservation system, nuclear cooling, vehicle thermal management, drug decrease, pasteurization, defense, spacecraft, cementitious materials and missiles, are more efficient than nanofluid practical application.

Initially, Niihara [7] investigated the rigidity and power of nanocomposite which was noticeably increased. Jana et al. [8] studied carbon nanotubes-gold nanoparticles and carbon nanotubes-copper nanoparticles with base fluid water, and they discovered that the hybrid has not improved thermal conductivity. Olthof et al. [9] done an experimental study made at high temperature, oxidation of vanadia spread on silicon dioxide, aluminum dioxide, titanium dioxide, hafnium dioxide, and zirconium dioxide. It showed an improvement in the crystallinity of V_2O_5 on SiO_2, mixed metal oxide appearance on ZrO_2, TiO_2 and polyvanadate species on Al_2O_3.

Afrand et al. [10] have shown at a solid volume fraction of 1% and with the temperature at 60^0C, the hybrid-nanofluid SiO_2-MWCNT/AE40 reached the maximum viscosity increment to 37.4% as a lubricant and as a coolant. Yang et al. [11] discussed alumina-zirconia/water and alumina- titania/water hybrid nanofluids. The findings stated that alumina-titania/water nanofluid showed a greater amount of heat transfer rate and a reduced friction factor than alumina-zirconia/water nanofluid. Their experimental data [12] matched well with the estimated Nusselt number and CNT-Fe_3O_4/water hybrid nanofluid friction factor. Xian et al. [13] and Sarkar [14] have reported about the affecting factors of hybrid nanofluid performance. Numerical evaluation of hybrid-nanofluids with nanoparticles Al_2O_3, TiO_2, and SiO_2, turbulent flow was evaluated by Minea [15].

Moldoveanu et al. [16] prepared the Al_2O_3-SiO_2 nanofluids and their hybrids. They measured the hybrid nanofluid viscosity variation with temperature. They found that increasing the temperature reduced the viscosity of hybrid nanofluid. Moldoveanu et al. [17] measured the viscosity of Al_2O_3-TiO_2 hybrid. The relative viscosity along volume fraction was connected by regression analysis for hybrid nanofluid and both nanofluids. They found their data fit well with experimental data. Abdul Hamid et al. [18] observed for various ratios of 1% volume concentration of SiO_2-TiO_2 hybrid with base fluid water and ethylene glycol (EG) mixture. Their conclusion disclosed optimum blend ratios for SiO_2-TiO_2 to enhance the dynamic viscosity and heat conductivity is 40:60 and 80:20.

Numerically Sahoo et al. [19] reported that the hybrid nanofluids were used as radiator coolant and Al_2O_3+Ag/water-based hybrid-nanofluid had high efficiency. Anjali Devi and Surya Uma Devi [20] studied and concluded that a heat transfer rate for hybrid nanofluid (Cu-Al_2O_3/water) was discovered elevated in the existence of a magnetic field. A new 3D model was hired by Hayat and Nadeem [21] their result showed that the hybrid nanofluid (Ag-CuO/water) has a higher heat transfer rate than nanofluid (CuO/water). Azwadi et al. [22] discussed those thermal physiognomies of hybrid nanofluids were sophisticated than nanofluids. Recently, Gorla et al. [23] studied numerically water-based hybrid-nanofluids with heat source/sink effects.

Kuznetsov [24] investigated the flow of nanofluid over a vertical surface of the natural convective boundary layer. Sheikoleslami et al. [25] studied the free convection heat transfer of nanofluid among a warm inner sinusoidal and a cold outer circular cylinder. Abdul Hakeem et al. [26] concluded that the reduced Nusselt number of metallic nanofluids was lower than non-metallic nanofluids in stretching and shrinking sheets with natural convection. A wonderful cluster of explores on the free convection of various geometries have been established in the papers of Ogulu et al.[27], Armaghani et al. [28], Makinde et al. [29], Sajjadi et al. [30], Alsabery et al. [31], Izadi et al.[32], Sheikholeslami et al.[33], Garoosi et al. [34], and Hady et al. [35].

Marangoni convection was induced by the variations of the surface tension gradients in the liquid-liquid or liquid-gas interfaces. Boundary layer flow of Marangoni convection has been received significant effect due to its wide range of applications in crystal growth melts, silicon wafer drying; stabilize soap film, welding, and convection. Marangoni flow appears in earth gravity furthermore in microgravity. The copious assessment of multiple geometries on Marangoni convection was carried out in the classical fluids job [36-40]. The relations between Marangoni number, Reynolds number, and Prandtl number were derived by Christopher et al. [41]. An excellent collection of works on Marangoni convection of nanofluids can be found in the papers of Aly and Ebaid [42], Arifin et al. [43] and [44], Lin et al. [45], Hamid and Arifin [46], and Remeli et al. [47]. Recently, Hayat et al. [48] have investigated the Marangoni mixed convection flow for Casson fluid over a permeable surface.

The study of hybrid nanofluid is still at its early stage. Oxide nanoparticles are preferred nanoparticles because of its resistance to oxidation together with lesser particle setting problems and it has a lower density than the metal density. Al_2O_3 has applications such as explosive additives, coatings, artillery, paints, and pigments. SiO_2 has the most conversant applications such as packaging, production of glass, drug delivery, gene delivery, cancer therapy and biosensors for DNA. TiO_2 has a wide range of applications such as food coloring, sunscreen lotion, polishes, and paint. Hence, by considering the advantages and applications of the aforementioned nanoparticles and the experimental studies in [16], [17] and [18] in the current investigation, the three different hybrid nanofluids such as Al_2O_3-SiO_2 /water, Al_2O_3-TiO_2 /water, and TiO_2-SiO_2 /water are considered and investigation is analytically made with Laplace transform upon a permeable flat surface under Marangoni convection.

As for the benefits of Laplace transform over other techniques, there are well-known solutions for many standardized second-order differential equations with variable coefficients, such as Bessel's equation, Kummer's equation, Legendre's equation, Airy's equation, etc. However, if the differential equation under account does not follow any of these kinds, we need to convert it. Otherwise, it is necessary to search for another solution method. Since most of the differential equations that we generally explore are forms that vary from those described above, Laplace transform is one of the best instruments to accomplish this job. Besides, the Laplace transform provides scientists with an opportunity to deduce an analytical solution in a closed-integral form.

2. Mathematical Formulation

A study is considered under two-dimensional, laminar, Marangoni boundary layer, the incompressible flow of hybrid nanofluid having a basis H_2O which containing a different type of hybrid nanoparticles Al_2O_3-SiO_2, Al_2O_3-TiO_2, and TiO_2 - SiO_2 past a flat surface with suction or injection or impermeable case. A Cartesian coordinate structure *(X, Y)* is presumed in which the X coordinate is evaluated along with the plate and the Y coordinate is evaluated normal to it, where the flow takes place at $Y \geq 0$. It is further considered that the temperature of the surface is $T_W(X)$, as shown in Fig. 1. The viscosity is considered to be temperature independent.

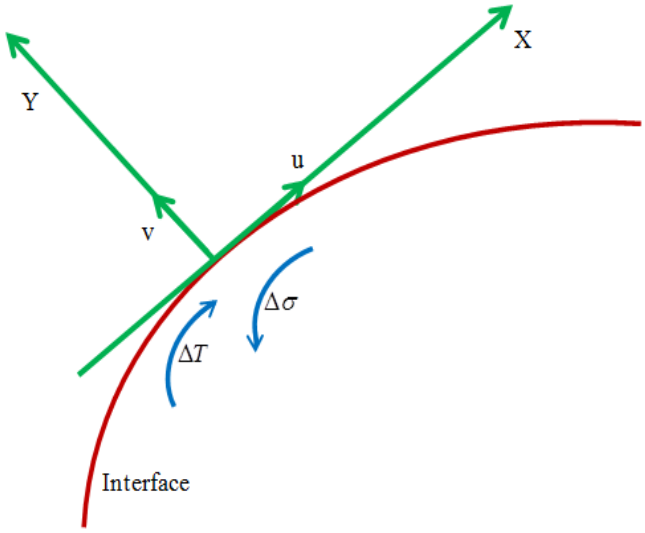

Fig. 1. Interface condition and coordinate system physical model

Under the above considerations, the governing equations are specified as Anjali Devi and Suriya Uma Devi [20] and Arifin et al. [43],

$$\frac{\partial u}{\partial x}+\frac{\partial v}{\partial y}=0 \tag{1}$$

$$u\frac{\partial u}{\partial x}+v\frac{\partial u}{\partial y}=\frac{\mu_{hnf}}{\rho_{hnf}}\frac{\partial^2 u}{\partial y^2} \tag{2}$$

$$u\frac{\partial T}{\partial x}+v\frac{\partial T}{\partial y}=\alpha_{hnf}\frac{\partial^2 T}{\partial y^2} \tag{3}$$

Subject to the boundary conditions

$$v=v_w, T=T_\infty+Ax^2, \mu_{hnf}\frac{\partial u}{\partial y}=\frac{\partial \sigma}{\partial T}\frac{\partial T}{\partial x} \quad \text{at} \quad y=0 \tag{4}$$

$$u\to 0, T\to\infty \quad \text{as} \quad y\to\infty \tag{5}$$

Here u and v are velocity components along the x and y axes, respectively. T is the temperature of the hybrid nanofluid. v_w is constant suction velocity. μ_{hnf} is the effective viscosity of hybrid nanofluid, ρ_{hnf} is the effective density of the hybrid nanofluid. α_{hnf} is the thermal diffusivity of the hybrid nanofluid and k_{hnf} is the effective thermal conductivity of hybrid nanofluid, which are given by Table 1 (Minea [15]).

Table 1. Thermophysical properties of nanoparticles and base fluid (Minea [15])

Property	Al_2O_3	SiO_2	TiO_2	Pure water
$C_p(J/kgK)$	765	703	692	4181
$\rho(kg/m^2)$	3970	2200	4175	996.5
$K(W/mK)$	40	1.2	8.4	0.613

Table 2. Hybrid nanofluid thermophysical properties (Anjali Devi and Suriya Uma Devi [20])

Thermophysical properties	Hybrid nanofluid
Density	$\rho_{hnf} = \{(1-\phi_2)[(1-\phi_1)]\rho_f + \phi_1\rho_{s_1}]\} + \phi_2\rho_{s_2}$
Heat capacity	$(\rho C_p)_{hnf} = \{(1-\phi_2)[(1-\phi_1)(\rho C_p)_f + \phi_1(\rho C_p)_{s_1}]\} + \phi_2(\rho C_p)_{s_2}$
Thermal conductivity	$\frac{k_{hnf}}{k_{nf}} = \frac{k_{s_2} + (n-1)k_{nf} - (n-1)\phi_2(k_{nf} - k_{s_2})}{k_{s_2} + (n-1)k_{nf} + \phi_2(k_{nf} - k_{s_2})}$ where $\frac{k_{nf}}{k_f} = \frac{k_{s_1} + (n-1)k_f - (n-1)\phi_1(k_f - k_{s_1})}{k_{s_1} + (n-1)k_f + \phi_1(k_f - k_{s_1})}$
Effective viscosity	$\mu_{hnf} = \frac{\mu_f}{(1-\phi_1)^{2.5}(1-\phi_2)^{2.5}}$
Thermal diffusivity	$\alpha_{hnf} = \frac{k_{hnf}}{(\rho C_p)_{hnf}}$

The hybrid nanoparticles and the base fluid are presumed as in thermal equilibrium and there is no slip between them. The temperature is thought to differ linearly with surface tension σ at the interface Chamkha et al. [49].

$$\sigma = \sigma_*(1-\gamma(T-T_*)) \tag{6}$$

where, σ_* is the surface tension at the interface T_∞ is the temperature of the ambient fluid and we considered that $T_* = T_\infty$. Along with temperature, for most liquids the surface tension σ declines. That means $\gamma > 0$ fluid property.

2.1. Hybrid nanofluid model and thermophysical properties

From Fig. 2 it is acclaimed that the relative viscosity for Al_2O_3-TiO_2 is correlated with the experimental results of Moldoveanu et al. [17]. Specifically, the hybrid nanofluid is plotted for different volume fractions such as 0.5%Al_2O_3-0.5%TiO_2, 0.5%Al_2O_3-1%TiO_2, and 0.5%Al_2O_3-1.5%TiO_2 gives a correlation with the existing experimental results. The simulation uses experimentally tested silicon dioxide (SiO_2) nanoparticles with a diameter of 20 nm [16], aluminum oxide (Al_2O_3) nanoparticles with a diameter of 43 nm [16], and titanium dioxide (TiO_2) with a diameter of 30 nm [17]. The theoretical model does not reflect the size of nanoparticle but it reflects the shape of the nanoparticle (n). An intense study on these characteristics should be carried out in the future in order to achieve a better correlation with experimental information.

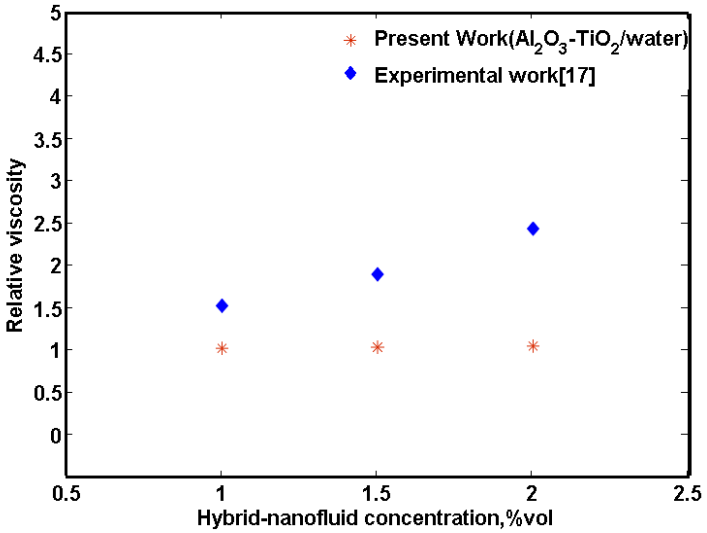

Fig. 2. Comparison graph

The thermophysical properties of hybrid nanofluid are listed in Table 2 (Anjali Devi and Suriya Uma Devi [20]). Suffix s_1 denotes solid nanoparticles and ϕ_1 is the solid volume fraction of Al_2O_3 in Al_2O_3-SiO_2/water and Al_2O_3-TiO_2/water

hybrid nanofluids and TiO_2 in TiO_2-SiO_2/water hybrid nanofluid, suffix s_2 denotes solid nanoparticles and ϕ_2 is the solid volume fraction of SiO_2 in Al_2O_3-SiO_2/water and TiO_2 -SiO_2/water hybrid nanofluids and TiO_2 in Al_2O_3-TiO_2/water hybrid nanofluid. Here $n=3$ is for spherical nanoparticles. μ_f, ρ_f are the viscosity, density of the base fluid (water) respectively and k_{nf} is the effective thermal conductivity of nanofluid. Hence, the thermophysical properties (Table 2) are chosen for three cases of hybrid nanofluids Al_2O_3-SiO_2/water, Al_2O_3-TiO_2/ water, and TiO_2-SiO_2/water. In our study at first, the nanoparticle volume fraction ϕ_1 of Al_2O_3in Al_2O_3-SiO_2/water, Al_2O_3-TiO_2/water and TiO_2 in TiO_2-SiO_2/water is fixed with 2.5%, and simultaneously nanoparticle volume fraction ϕ_2 of SiO_2 in Al_2O_3-SiO_2/water, TiO_2-SiO_2/water, and TiO_2 in Al_2O_3-TiO_2/water is fixed with 0.5%.

3. Similarity Transformation

To get a similarity solution of equations (1)-(3) with the boundary condition equation (4) and equation (5) of the succeeding form, (see Sastry et al. [38])

$$\psi(\eta)=\varsigma_2 x f,\ \theta=\frac{(T-T_\infty)}{Ax^2} \text{ and } \eta=\varsigma_1 y \tag{7}$$

where $u=\partial\psi/\partial y$ and $v=-\partial\psi/\partial x$, ψ is the stream function. Additionally, $A,\varsigma_1,\varsigma_2$ are constants given by,

$$A=\frac{\Delta T}{L^2},\ \varsigma_1=\left(\frac{\sigma_*\gamma A\rho_f}{\mu_f{}^2}\right)^{1/3} \text{ and } \varsigma_2=\left(\frac{\sigma_*\gamma A\mu_f}{\rho_f{}^2}\right)^{1/3} \tag{8}$$

with ΔT be the constant characteristic temperature and L be the surface length. By substituting equations (7) and (8) in equations (2) and (3), the obtained ordinary differential equations as,

$$f'''+(1-\phi_1)^{2.5}(1-\phi_2)^{2.5}[(1-\phi_2)((1-\phi_1)+\phi_1\rho_{s_1}/\rho_f)+\phi_2\rho_{s_2}/\rho_f](ff''-f'^2)=0 \tag{9}$$

$$\theta''+\frac{k_f}{k_{hnf}}\Pr\left\{(1-\phi_2)[1-\phi_1+\phi_1\frac{(\rho C_p)_{s_1}}{(\rho C_p)_f}]+\phi_2\frac{(\rho C_p)_{s_2}}{(\rho C_p)_f}\right\}(f\theta'-2f'\theta)=0 \tag{10}$$

and the boundary conditions are transformed as,

$$f=f_w, f''(0)=-2(1-\phi_1)^{2.5}(1-\phi_2)^{2.5}, \theta(0)=1 \tag{11}$$

$$f'(\infty)\to 0, \theta(\infty)\to 0 \tag{12}$$

where Pr is the Prandtl number, f_w is the wall mass transfer parameter ($f_w>0$ suction, $f_w=0$ impermeable and $f_w<0$ injection (or) blowing parameter). The surface velocity $u(X,0)=u_w(X)$ is given forth as (see Aly and Ebaid [42])

$$u_w(x)=\left(\frac{(\sigma_*\gamma A)^2}{\rho_f\mu_f}\right)^{1/3} x f'(0) \tag{13}$$

Another important characteristic of the present investigation is the Nusselt number which is given by Lin et al. [45]

$$Nu_x=-\left(\frac{K_{hnf}}{K_f}\right)\varsigma_1 x\theta'(0) \tag{14}$$

The average Nusselt number depends on the average temperature difference across the temperature of the surface and the temperature far from the surface (ambient fluid) is given by Arifin et al. [44]. Now the hybrid nanofluid average Nusselt number is given by,

$$Nu_L=-\left(\frac{K_{hnf}}{K_f}\right)Ma_L^{1/3}\ \Pr^{1/3}\ \theta'(0) \tag{15}$$

where Ma_L is the Marangoni number based on L and defined as (see Sastry et al. [38])

$$Ma_L=\frac{\sigma_* AL^2}{\mu_f\alpha_f}=\frac{\sigma_*\Delta TL}{\mu_f\alpha_f} \tag{16}$$

The Reynold's number obtained from Christopher and Wang [41] identified regarding the surface velocity are related to the Marangoni number and is given as,

$$\mathrm{Re}_L = \frac{u(x,0)L}{\upsilon_f} = f'(0)Ma_L^{2/3}\,\mathrm{Pr}^{-2/3} \tag{17}$$

4. Analytical Solution

4.1 Analytical Solution of velocity $f(\eta)$

Concerning the conditions of $f(\eta)$ in equation (11) and equation (12), it can be deduced as

$$f(\eta) = a_1 + a_2 e^{-\alpha\eta} \tag{18}$$

where $a_1 = f_w - a_2$, $a_2 = -(2/\alpha^2)(1-\phi_1)^{2.5}(1-\phi_2)^{2.5}$. By substituting equation (18) and its derivative in equation (9), we get

$$-\alpha^3 a_2 e^{-\alpha\eta} + (1-\phi_1)^{2.5}(1-\phi_2)^{2.5}\left\{(1-\phi_2)[1-\phi_1+\phi_1\frac{\rho_{s_1}}{\rho_f}]+\phi_2\frac{\rho_{s_2}}{\rho_f}\right\}\left\{(a_1+a_2e^{-\alpha\eta})(\alpha^2 a_2 e^{-\alpha\eta})+(\alpha a_2 e^{-\alpha\eta})^2\right\}=0 \tag{19a}$$

Dividing throughout the above equation by $a_2 e^{-\alpha\eta}$ and using equation (18), we get

$$\alpha^3 - (1-\phi_1)^{2.5}(1-\phi_2)^{2.5} B_1 f_w \alpha^2 - 2((1-\phi_1)^{2.5}(1-\phi_2)^{2.5})^2 B_1 = 0 \tag{19b}$$

where

$$B_1 = (1-\phi_2)[(1-\phi_1+\phi_1\frac{\rho_{s_1}}{\rho_f}]+\phi_2\frac{\rho_{s_2}}{\rho_f} \tag{19c}$$

In our study, MATLAB R2015a has been used to find the roots of equation (19). The non-negative solution of equation (19) is only to be assumed to get the solution. For a lot of details regarding deducing the precise solutions of $f(\eta)$ during this section, the reader is suggested to visualize the subsequent papers by Aly and Vajravelu [50] and Aly and Ebaid [51].

4.2 Analytical Solution of temperature $\theta(\eta)$

Here Laplace transform is applied to solve the energy equation (10) and the boundary conditions (11) and (12). Assume that $t = -e^{-\alpha\eta}$ including equation (18), we get

$$\frac{\alpha^2}{\left\{(1-\phi_2)[1-\phi_1+\phi_1\frac{(\rho C_p)_{s_1}}{(\rho C_P)_f}]+\phi_2\frac{(\rho C_p)_{s_2}}{(\rho C_P)_f}\right\}}(2t\theta_t + t^2\theta_{tt}) + \frac{k_f}{k_{hnf}}\mathrm{Pr}\left\{(a_1+a_2e^{-\alpha\eta})(-\alpha t\theta_t)+2\alpha a_2 e^{-\alpha\eta}\theta\right\}=0 \tag{20a}$$

$$2\theta_t + t\theta_{tt} + B_3\left\{\left(\frac{-f_w}{\alpha}-\frac{2}{\alpha^3}(1-\phi_1)^{2.5}(1-\phi_2)^{2.5}(1-t)\right)\theta_t + \frac{4}{\alpha^3}(1-\phi_1)^{2.5}(1-\phi_2)^{2.5}\theta\right\}=0 \tag{20b}$$

where

$$B_3 = \frac{k_f}{k_{hnf}}\mathrm{Pr}\,B_2 \text{ and } B_2 = (1-\phi_2)\left\{[1-\phi_1+\phi_1\frac{(\rho C_p)_{s_1}}{(\rho C_p)_f}]+\phi_2\frac{(\rho C_p)_{s_2}}{(\rho C_p)_f}\right\} \tag{20c}$$

Finally, we have

$$t\theta_{tt} + (a-bt)\theta_t + 2b\theta(t) = 0 \tag{21a}$$

where

$$a = 2 - \frac{B_3}{\alpha}(f_w + \frac{2}{\alpha^2}(1-\phi_1)^{2.5}(1-\phi_2)^{2.5}) \text{ and } b = \frac{2B_3}{\alpha^3}(1-\phi_1)^{2.5}(1-\phi_2)^{2.5} \tag{21b}$$

Subject to the boundary conditions

$$\theta(0^-) = 0, \theta(-1) = 1 \tag{22}$$

By using the transform of Laplace to the equation (21), it becomes

$$L[t\theta''(t)]+L[(a-bt)\theta_t]+L[2b\theta(t)]=0$$
$$-2s\Theta(s)-s^2\Theta'(s)+as\Theta(s)+3b\Theta(s)+ms\Theta'(s)=0 \tag{23}$$

$$(b-s)s\Theta'(s)+((a-2)s+3b)\Theta(s)=0 \tag{24}$$

where $\Theta(s)$ is the Laplace transform of $\theta(t)$. Now on integrating equation (24), we obtain

$$\int\frac{\Theta'(s)}{\Theta(s)}ds=\int\frac{(a-2)s+3b}{s(s-b)}ds \tag{25a}$$

$$\log_e\Theta(s)=(a-2)\log_e(s-b)-3\log_e s+3\log_e(s-b)+\log_e C \tag{25b}$$

$$\Theta(s)=\frac{C}{(s-b)^{-a-1}s^3} \tag{26}$$

Now, C is integration constant to be found and using inverse transform of Laplace, equation (26) becomes

$$L^{-1}\{\Theta(s)\}=L^{-1}\left\{\frac{C}{(s-b)^{-a-1}s^3}\right\} \tag{27}$$

$$\theta(t)=\frac{C}{2(-a-2)!}\int_0^t(t-\mu)^2\mu^{-a-2}e^{b\mu}d\mu \tag{28}$$

By applying the limit condition $\theta(-1)=1$ gives

$$C=\frac{2\Gamma(-a-1)}{\int_0^{-1}(1+\mu)^2\mu^{-a-2}e^{b\mu}d\mu} \tag{29}$$

Hence by the value of the C equation (28) becomes

$$\theta(t)=\frac{2\Gamma(-a-1)\int_0^t(t-\mu)^2\mu^{-a-2}e^{b\mu}d\mu}{2\Gamma(-a-1)\int_0^{-1}(1+\mu)^2\mu^{-a-2}e^{b\mu}d\mu} \tag{30}$$

Carrying out the equation (30) integrations, we attain the final analytical solution for $\theta(t)$ with regard to the generalized incomplete gamma function

$$\theta(t)=\frac{b^2t^2\Gamma(-a-1,0,bt)-2bt\Gamma(-a,0,bt)+\Gamma(-a+1,0,bt)}{b^2\Gamma(-a-1,0,b)-2b\Gamma(-a,0,b)+\Gamma(-a+1,0,b)} \tag{31}$$

The exact solution with respect to η can be framed as

$$\theta(\eta)=\frac{b^2e^{-2a\eta}\Gamma(-a-1,0,be^{-a\eta})-2be^{-a\eta}\Gamma(-a,0,be^{-a\eta})+\Gamma(-a+1,0,be^{-a\eta})}{b^2\Gamma(-a-1,0,b)-2b\Gamma(-a,0,b)+\Gamma(-a+1,0,b)} \tag{32}$$

Table 3. Values of $f''(0)$ for various values of solid volume fraction with $\Pr=6.2$ and $f_w=0$

ϕ_1	ϕ_2	Sastry et al.[38]	Hamid and Arifin [46]	Present work
0	0	-2	-2	-2
0.1	0	-1.5368669	-1.5368669	-1.5368669
0.2	0	-1.1448668	-1.1448668	-1.1448668

5. Results and Discussion

Marangoni convection boundary layer flow of three distinct hybrid nanofluids, namely, Al_2O_3-SiO_2/water, Al_2O_3-TiO_2/water, and TiO_2-SiO_2/water, with heat and wall mass transfer effects past a flat surface is discussed for the cases of suction, impermeable and injection(blowing). The ordinary differential equations with the boundary conditions are

solved by Laplace transform. By using derivatives of equation (18) for $f'(\eta)$ and equation (32) for $\theta(\eta)$ in MATLAB R2015a software, the graphical results were plotted for velocity and temperature profiles respectively. Tables and plots were drawn to give a picture of the validation and impact of the parameters, mainly solid volume fractions (ϕ_1 and ϕ_2) and wall mass transfer (f_w). In the present study, the cases of suction ($f_w > 0$ and is dosed as $f_w = 1$) with black color, impermeable ($f_w = 0$) with green color and injection ($f_w < 0$ and is dosed as $f_w = -1$) with red color are plotted in the graph. The base fluid water Prandtl number (Pr) is fixed as 6.2. The comparison is made between the current results through Sastry et al. [38] and Hamid and Arifin [46] to validate the used system and it is shown in Table 3.

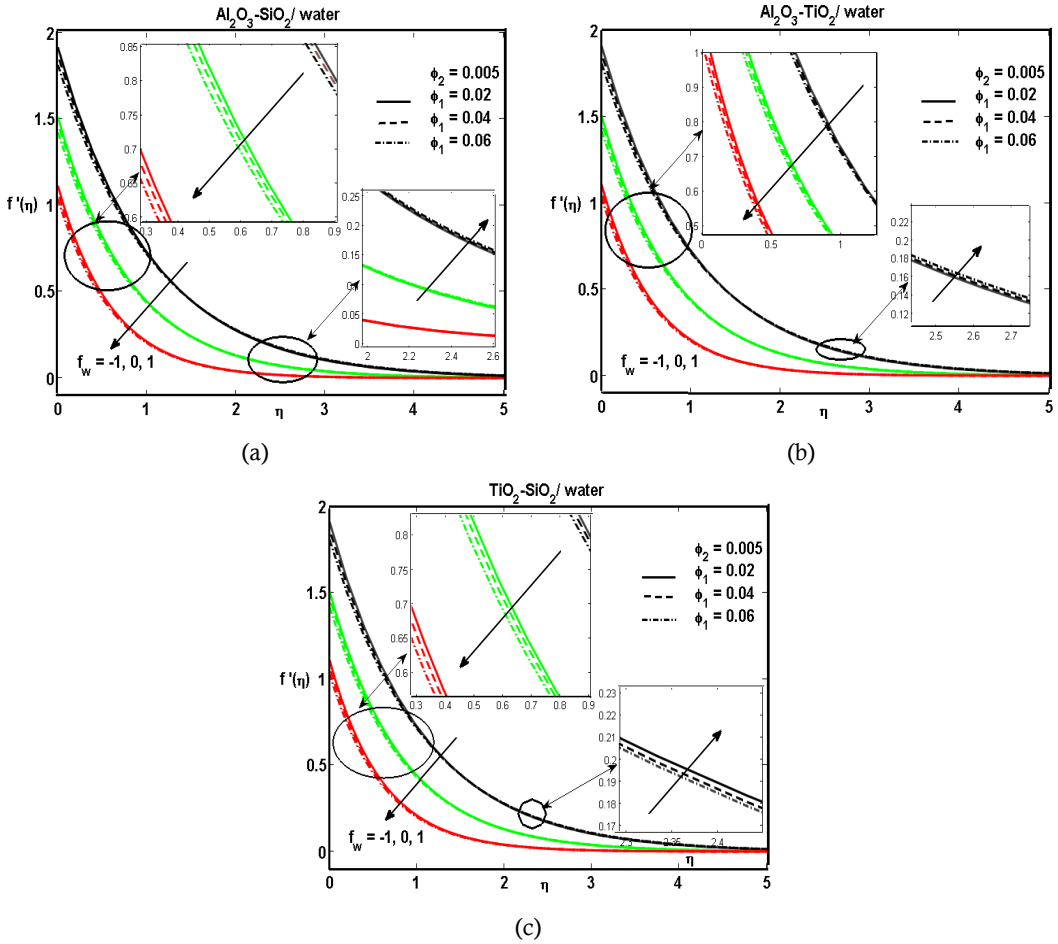

Fig. 3. Effects of velocity profiles for various values of ϕ_1 and f_w with $\Pr = 6.2$, $\phi_2 = 0.005$

a) Al_2O_3-SiO_2/water, b) Al_2O_3-TiO_2/water and c) TiO_2-SiO_2/water

Figure 3(a-c) elucidates the effect of the solid volume fraction ϕ_1 of Al_2O_3 in Al_2O_3-SiO_2/water, Al_2O_3-TiO_2/water in Figure 3a and Figure 3b respectively and for TiO_2 in TiO_2-SiO_2/water in Figure 3c of hybrid nanofluids for three cases of wall mass transfer parameter (f_w) (injection, impermeable and suction). While improving the velocity profile values of ϕ_1 all the three hybrid nanofluids is declining. Physically speaking, hybrid nanoparticles inclusion in the base fluid offers resistance, and this occurs because of their density relatively higher than the base fluid. The velocity profile slightly increases after $\eta = 1$ for impermeable ($f_w = 0$) and injection ($f_w = -1$) cases. This is because the increase in the volume fraction of nanoparticles increases the power exchange rates. Hence the movements of particles become irregular and random. For injection ($f_w = -1$) case when rises the solid volume fraction (ϕ_1), the velocity profile declines throughout the fluid motion. Also, while increasing the wall mass transfer parameter (f_w), Al_2O_3-SiO_2/water, Al_2O_3-TiO_2/water, and TiO_2-SiO_2/water hybrid nanofluids retard similarly.

Figure 4(a-c) represents the dimensionless velocity for the various values of solid volume fraction ϕ_2 for SiO_2 in two-hybrid nanofluids Al_2O_3-SiO_2/water (Figure 4a), TiO_2-SiO_2/water (Figure 4c), and TiO_2 in Al_2O_3-TiO_2/water (Figure 4b). While increasing the solid volume fraction ϕ_2 from 0.005 to 0.04 the velocity profile retards near the wall and has opposite effect for Al_2O_3-SiO_2/water(Figure 4a) and TiO_2-SiO_2/water(Figure 4c) for three cases of wall mass transfer parameter (f_w), namely injection, impermeable and suction cases which may be caused by more interactions between confined nanoparticles. But especially the hybrid nanofluid Al_2O_3-TiO_2/ water have significant opposite effect only for injection case, since the density of TiO_2 is higher than SiO_2.

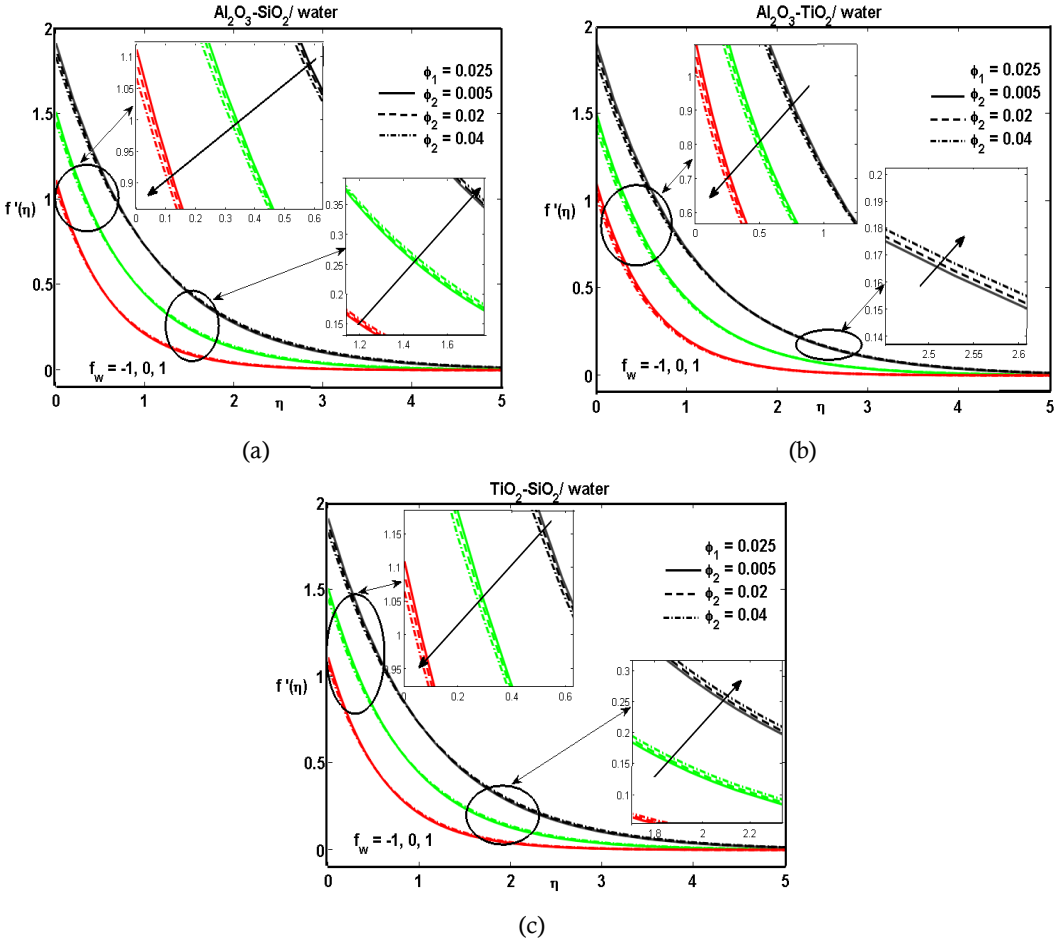

Fig. 4. Effects of velocity profiles for various values of ϕ_2 and f_w with $\mathrm{Pr} = 6.2$, $\phi_1 = 0.025$
a) Al_2O_3-SiO_2/water, b) Al_2O_3-TiO_2/water and c) TiO_2-SiO_2/water

The velocity distribution for various equal solid volume fractions of hybrid nanoparticles $\phi_1 = \phi_2$ for Al_2O_3-SiO_2/water (Figure 5a), Al_2O_3-TiO_2/water (Figure 5b) and TiO_2-SiO_2/water (Figure 5c) is shown in Figure 5. The simultaneous increase of the values of solid volume fractions of both the nanoparticles of hybrid nanofluid diminishes the velocity profile. The drop in the distribution with the solid volume fraction and ϕ_2 indicate that the overall drag increases. The inverse influence in the velocity distribution is observed after $\eta = 1$ for Al_2O_3-SiO_2/water, Al_2O_3-TiO_2/water and TiO_2-SiO_2/water for all the cases of wall mass transfer parameter as suction, injection and impermeable except Al_2O_3-TiO_2/water suction case. Figures 5a, 5b, and 5c show the notable increase in the boundary layer thickness which has been observed in the case of suction than in the cases of impermeable and injection. The problem of suction ($f_w = 1$) at the surface has the propensity to decline the fluid velocity, though the surface injection $(f_w = -1)$ and impermeable ($f_w = 0$) cases create a contrary effect, specifically rise the fluid velocity.

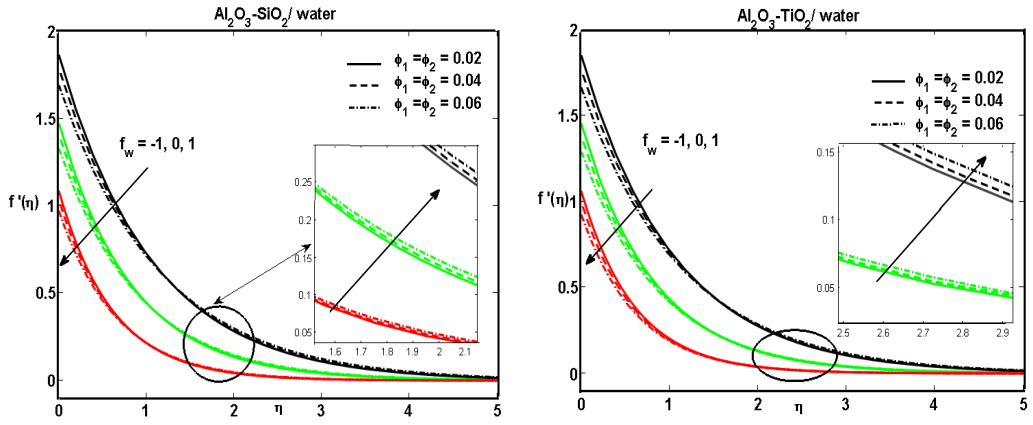

Fig. 5. Effects of velocity profiles for various values of $\phi_1 = \phi_2$ and f_w with $\mathrm{Pr} = 6.2$

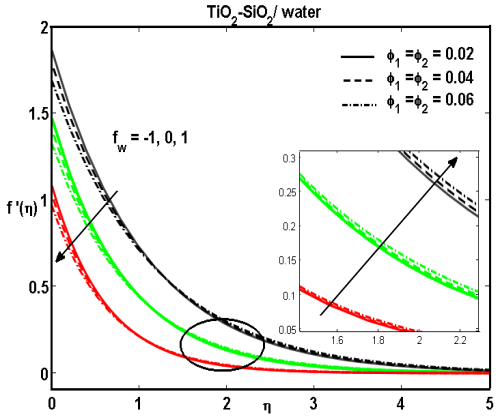

(c)

Fig. 5. Effects of velocity profiles for various values of $\phi_1 = \phi_2$ and f_w with $\Pr = 6.2$
a) Al_2O_3-SiO_2/water, b) Al_2O_3-TiO_2/water and c) TiO_2-SiO_2/water

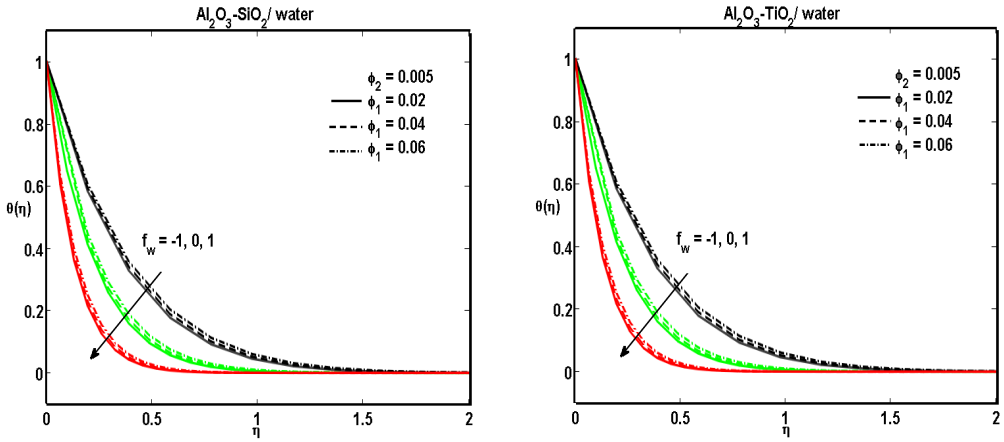

(a) (b)

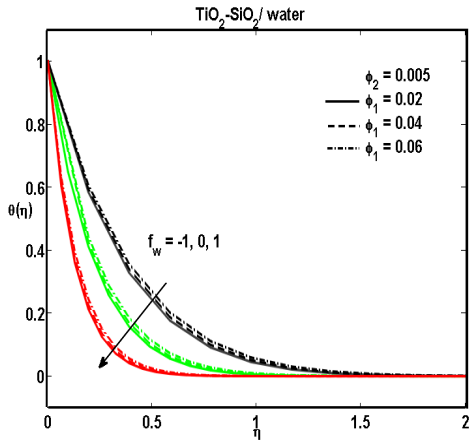

(c)

Fig. 6. Effects of temperature profiles for various values of ϕ_1 and f_w with $\Pr = 6.2$, $\phi_2 = 0.005$
a) Al_2O_3-SiO_2/water, b) Al_2O_3-TiO_2/water and c) TiO_2-SiO_2/water

It is worth mentioning that the volume fraction of hybrid nanoparticles could be a key parameter for finding out the impact of hybrid nanoparticles on temperature distributions. Figure 6 illustrates the escalating temperature distribution of hybrid nanofluids with respect to the different solid volume fraction ϕ_1 of Al_2O_3 in Al_2O_3-SiO_2/water (Figure 6a) and Al_2O_3-TiO_2/water (Figure 6b) and TiO_2 in TiO_2-SiO_2/water (Figure 6c). This is because of the circumstances that the hybrid nanoparticles have lesser specific heat and greater thermal conductivity parallel to the base fluid (water). Hence, all three hybrid nanofluids raise the temperature profile. The increase in wall mass transfer (f_w) declines the temperature distribution. Since in the instance of increasing f_w, the fluid is carried closer to the surface and declines the thermal boundary layer thickness.

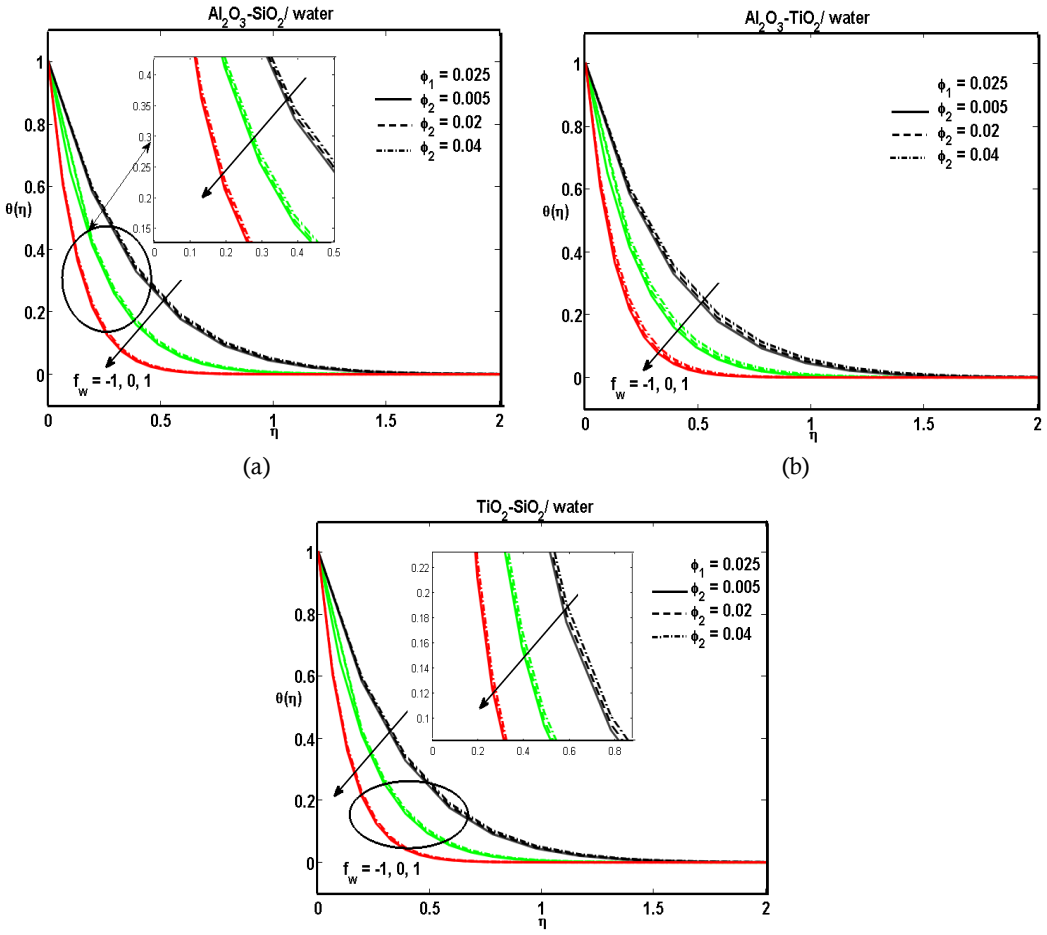

Fig. 7. Effects of temperature profiles for various values of ϕ_2 and f_w with $\mathrm{Pr} = 6.2$, $\phi_1 = 0.025$
a) Al_2O_3-SiO_2/water, b) Al_2O_3-TiO_2/water and c) TiO_2-SiO_2/water

The effect of solid volume fraction ϕ_2 on the temperature profile for $f_w = -1$, $f_w = 0$ and $f_w = 1$ are plotted in Figure 7. It is noted that a rise in ϕ_2 of SiO_2 in Al_2O_3-SiO_2/water and TiO_2-SiO_2/water in Figure 7a and Figure 7c independently and TiO_2 of Al_2O_3-TiO_2/water in Figure 7b yields an increase in the hybrid nanofluid temperature. While comparing for an increment of solid volume fraction SiO_2 the energy field rise in Figure 7b is higher than Figure 7a and Figure 7c. This is because the heat conductivity of TiO_2 is higher than that of SiO_2. The thermal boundary layer turns slenderer for injection ($f_w = -1$) and denser for suction ($f_w = 1$) while balanced with impermeable ($f_w = 0$) surface for all the three hybrid nanofluids. The result is compatible with physical parameters.

Figure 8 portrays the variation of equal solid volume fraction when $\phi_1 = \phi_2$ and wall mass transfer (f_w) regarding the temperature field. The temperature profile increases while increasing the values of solid volume fraction of both the nanoparticles at the same time for the hybrid nanofluids Al_2O_3-SiO_2/water, Al_2O_3-TiO_2/water and TiO_2-SiO_2/water in Figure 8a, Figure 8b and Figure 8c, respectively. As the volume fraction of hybrid nanoparticles increases, the movement of particles becomes irregular and random due to an increment in the rate of energy transfer throughout the fluid which hikes the temperature profile. The increase in temperature distribution of Al_2O_3-SiO_2/water (Figure 8a) and TiO_2-SiO_2/water (Figure 8c) hybrid nanofluids are lower than Al_2O_3-TiO_2/water (Figure 8b) hybrid nanofluid. At the same time rising the wall mass transfer (f_w) decline the temperature profile for the three hybrid nanofluids. We can see that for all the three hybrid nanoparticles considered, the suction parameter tends to lower the energy of the flow field while the injection parameter raises the energy field for the various values of $\phi_1 = \phi_2$.

Table 4. Comparison of results for $f''(0)$ when $\phi_1 = 2.5\%$ and $\phi_2 = 0.5\%$

Parameters	Values	Al_2O_3-SiO_2/water		Al_2O_3-TiO_2/water		TiO_2-SiO_2/water	
		Analytical	Numerical	Analytical	Numerical	Analytical	Numerical
f_w	-1	1.910634	1.910576	1.907236	1.907142	1.908873	1.908796
	-0.5	1.712229	1.712175	1.708296	1.708202	1.710191	1.710117
	0	1.508484	1.508449	1.503949	1.503867	1.506136	1.506076
	0.5	1.305072	1.305057	1.299942	1.299874	1.302416	1.302373
	1	1.111272	1.111268	1.105702	1.105639	1.108388	1.108353

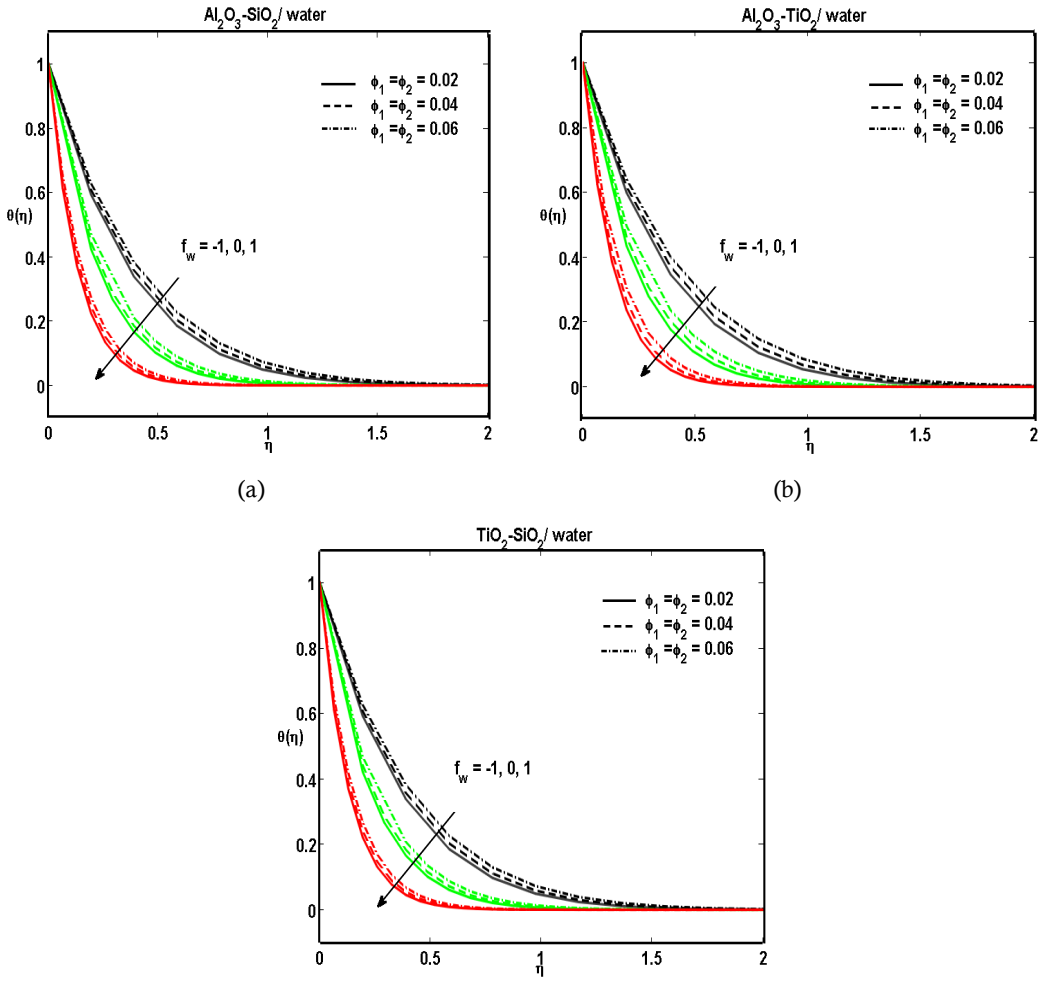

Fig. 8. Effects of temperature profiles for various values of $\phi_1 = \phi_2$ and f_w with $\Pr = 6.2$
a) Al_2O_3-SiO_2/water, b) Al_2O_3-TiO_2/water and c) TiO_2-SiO_2/water

Table 5. The influence of the wall mass transfer (f_w) on $-\theta'(0)$ for the three hybrid nanofluids, $\Pr = 6.2, \phi_1 = 2.5\%$ and $\phi_2 = 0.5\%$.

f_w	Al_2O_3-SiO_2/ water	Al_2O_3-TiO_2/ water	TiO_2-SiO_2/ water
-1	2.69136	2.68224	2.69561
-0.75	2.98667	2.97503	2.99278
-0.5	3.3549	3.33994	3.36383
-0.25	3.81158	3.79234	3.82456
0	4.37016	4.34561	4.38876
0.25	5.0381	5.00729	5.06399
0.5	5.81694	5.77905	5.85176
0.75	6.70172	6.65613	6.74692
1	7.68253	7.62882	7.73929

Table 4 shows the comparison between Laplace transform and Runge-Kutta Fehlberg results on the analytical and numerical values respectively of the surface velocity $f''(0)$ for various values of f_w for the three hybrid nanofluids Al_2O_3-SiO_2/water, Al_2O_3-TiO_2/water, and TiO_2-SiO_2/water and observed a good agreement. It is confirmed from the table that the hiking values of f_w lowering the surface velocity. Among the three hybrid nanofluids Al_2O_3-TiO_2/water hybrid nanofluid have the lower surface velocity and Al_2O_3-SiO_2/water hybrid nanofluid have the higher surface velocity than TiO_2-SiO_2/water hybrid nanofluid.

Table 5 gives the calculation to investigate the influences of the heat transfer rate. It is clear from Table 5 that the increase of values of wall mass transfer parameter while fixing the Prandtl number and solid volume fraction of hybrid nanoparticles heat transfer rate increases for the three hybrid nanofluids. While relating the heat transfer rate of the three hybrid nanofluids, TiO_2-SiO_2/water has higher and Al_2O_3-TiO_2/water has lower than Al_2O_3-SiO_2/water heat transfer rate.

6. Conclusion

The current investigation was on the three different hybrid nanofluids past a permeable flat surface with suction, injection and impermeable together with Marangoni convection. The analytical results were presented for the solid volume fraction of the nanoparticles and wall mass transfer parameter for Aluminium oxide-Silicon dioxide/water, Aluminium oxide-Titanium dioxide/water and Titanium dioxide-Silicon dioxide/water. The following significant conclusions achieved from the present exploration for the physical parameters.

- The effect of solid volume fraction is decelerating the velocity distribution for all the three hybrid nanofluids in the cases of suction, impermeable and injection.
- The temperature rises with the increment of solid volume fraction for all the hybrid nanofluids.
- The increment of wall mass transfer parameter declines the velocity distribution and energy field for Aluminum oxide-Silicon dioxide/water, Aluminum oxide-Titanium dioxide/water, and Titanium dioxide-Silicon dioxide/water hybrid nanofluids.
- Among the three hybrid nanofluids Al_2O_3-TiO_2/water hybrid nanofluid has lower surface velocity, and heat transfer rate in the presence of suction, injection and impermeable cases.
- Al_2O_3-SiO_2/water has higher surface velocity and TiO_2-SiO_2/water has the higher heat transfer rate than Al_2O_3-TiO_2/water hybrid nanofluid.

Author Contributions

Author 1 planned the scheme, initiated the project and suggested the experiments; Author 2 conducted the experiments and analyzed the empirical results; Author 3 developed the mathematical modeling and examined the theory validation. The manuscript was written through the contribution of all authors. All authors discussed the results, reviewed and approved the final version of the manuscript.

Acknowledgments

Not applicable.

Conflict of Interest

The authors declared no potential conflicts of interest with respect to the research, authorship and publication of this article.

Funding

The authors received no financial support for the research, authorship and publication of this article.

Data Availability Statements

The datasets generated and/or analyzed during the current study are available from the corresponding author on reasonable request.

Nomenclature

A	Constant	ψ	Stream function, $m^2.s^{-1}$
C_P	Specific heat, $J.Kg.K^{-1}$	ϕ_1	Solid volume fraction of first nanoparticle of hybrid nanofluid
f	Stream function similarity variable		
f_W	Wall mass transfer	ϕ_2	Solid volume fraction of second nanoparticle of hybrid nanofluid
k	Thermal conductivity, $W.m^{-1}.K^{-1}$		
L	Surface length, m	ν	Kinematic viscosity, $m^2.s^{-1}$
Ma	Marangoni number	γ	Positive fluid property
Nu_L	Average Nusselt number	μ	Effective viscosity, $N.s.m^{-2}$
Nu_x	Local Nusselt number	η	Similarity variable
Pr	Prandtl number	ρ	Density, $Kg.m^{-3}$
Re_L	Reynolds number	ς_1 , ς_2	Similarity transformation coefficients
T	Temperature, K	θ	Temperature similarity variable
ΔT	Characteristic temperature, K	***Subscripts***	
$T_W(X)$	Temperature of the surface, K	s_1	Solid nanoparticle of first nanoparticle
u	x component of velocity, $m.s^{-1}$	s_2	Solid nanoparticle of second nanoparticle

v	y component of velocity, $m.s^{-1}$	nf	Nanofluid
x	Cartesian coordinate along the interface, m	hnf	Hybrid nanofluid
y	Cartesian coordinate normal to the interface, m	f	Fluid
Greek letters		w	Wall
α	Thermal diffusivity, $m^2.s^{-1}$	*	Interface
σ	Surface tension, $N.m^{-1}$	∞	For away from the surface

References

[1] Choi, S.U.S., Enhancing thermal conductivity of fluids with nanoparticle, *The Proceedings of the 1995 ASME International Mechanical Engineering Congress and Exposition, San Francisco,* ASME, FED 231/MD66, USA, 1995, 99-105.

[2] Kulkarni, D.P., Debendra, K.D., Ravikanth S.V., Application of nanofluids in heating buildings and reducing pollution, *Applied Energy*, 86, 2009, 2566-2573.

[3] Razali, A.A., Sadikin, A., Ayop, S.S., Structural analysis and morphological study of Al_2O_3 nanofluids in microchannel heat sink, *Journal of Advanced Research in Fluid Mechanics and Thermal Sciences*, 46(1), 2018, 139-146.

[4] Shen, B., Shih, A.J., Tung, S.C., Application of nanofluids in minimum quantity lubrication grinding, *Tribology Transactions*, 51, 2008, 730-737.

[5] Xuan, Y., Li, Q., Investigation on convective heat transfer and flow features of nanofluids, *Journal of Heat Transfer*, 125**,** 2003, 151-155.

[6] Abu-Nada, E., Application of nanofluids for heat transfer enhancement of separated flows encountered in a backward facing step, *International Journal of Heat and Fluid Flow*, 29, 2008, 242-249.

[7] Niihara, K., New design concept of structural ceramics- ceramic nanocomposites, *The Centennial Memorial Issue of The Ceramic Society of Japan*, 99(10), 1991, 974-982.

[8] Jana, S., Salehi-Khojin, A., Zhong, W.H., Enhancement of fluid thermal conductivity by the addition of single and hybrid nano-additives, *Thermochimica Acta*, 462, 2007, 45-55.

[9] Olthof, B., Khodakov, A., Bell, A.T., Iglesia, E., Effects of support composition and pretreatment conditions on the structure of vanadia dispersed on SiO_2, Al_2O_3, TiO_2, ZrO_2 and HfO_2, *The Journal of Physical Chemistry B*, 104, 2000, 1516-1528.

[10] Afrand, M., Najafabadi, K.N., Akbari, M., Effects of temperature and solid volume fraction on viscosity of SiO_2-MWCNTs/SAE40 hybrid nanofluid as a coolant and lubricant in heat engines, *Applied Thermal Engineering*, 102, 2016, 45-54.

[11] Yang, C., Wu, X., Zheng, Y., Qiu, T., Heat transfer performance assessment of hybrid nanofluids in a parallel channel under identical pumping power, *Chemical Engineering Science,* 168, 2017, 67–77.

[12] Syam Sundar, L., Sousa, Antonio C. M., Singh, M.K., Heat transfer enhancement of low volume concentration of carbon nanotube Fe_3O_4/ Water hybrid nanofluids in a tube with twisted tape inserts under turbulent flow, *Journal of Thermal Science and Engineering Applications*, 7(021015), 2015, 1-12.

[13] Xian, H.W., Sidik, N.A.C., Aid, S.R., Ken, T.L., Asako, Y., Review on preparation techniques, properties and performance of hybrid nanofluid in recent engineering applications, *Journal of advanced Research in Fluid Mechanics and Thermal Sciences,* 45 (1), 2018, 1-13.

[14] Sarkar, J., Ghosh, P., Adil, A., A review on hybrid nanofluids: Recent research, development and applications, *Renewable and Sustainable Energy Reviews,* 43, 2015, 164-177.

[15] Minea A.A., Hybrid nanofluids based on Al_2O_3, TiO_2 and SiO_2: Numerical evaluation of different approaches, *International Journal of Heat Mass Transfer*, 104, 2017, 852– 860.

[16] Moldoveanu, G.M., Ibanescu, C., Danu, M., Minea, A.A., Viscosity estimation of Al_2O_3, SiO_2 nanofluids and their hybrid: An experimental study, *Journal of Molecular Liquids*, 2018, 253, 2018, 188-196.

[17] Moldoveanu, G.M., Minea, A.A., Iacob, M., Ibanescu, C., Danu, M., Experimental study on viscosity of stabilized Al_2O_3,TiO_2 nanofluids and their hybrid, *Thermochimica Acta*, 659, 2018, 203-212.

[18] Abdul Hamid, K., Azmi, W.H., Nabil, M.F., Mamat, R., Sharma, K.V., Experimental investigation of thermal conductivity and dynamic viscosity on nanoparticle mixture ratios of TiO_2-SiO_2 nanofluids, *International Journal of Heat and Mass Transfer*,116, 2018, 1143-1152.

[19] Sahoo, R.R., Ghosh, P., Sarkar, J., Performance analysis of a louvered fin automotive radiator using hybrid nanofluid as coolant, *Heat Transfer-Asian Research,* 46(7), 2017, 978-995.

[20] Anjali Devi, S.P., Suriya Uma Devi, S., Numerical investigation of hydromagnetic hybrid Cu-Al_2O_3/water nanofluid flow over a permeable stretching sheet with suction, *International Journal of Nonlinear Sciences and Numerical Simulation*, 17(5), 2016, 249-257.

[21] Hayat, T., Nadeem, S., Heat transfer enhancement with Ag-CuO/water hybrid nanofluid, *Results in Physics*, 7, 2017, 2317-2324.

[22] Azwadi, C.S.N., Adamu, I.M., Jamil, M.M., Preparation methods and thermal performance of hybrid nanofluids, *Journal of Advanced Review on Scientific Research*, 24(1), 2016, 13-23.

[23] Gorla, R.S.R., Mansour, M.A., Rashad, A.M., Salah, T., Heat source/sink effects on a hybrid nanofluid-filled porous cavity, *Journal of Thermophysics and Heat Transfer,* 31(4), 2017, 1-11.

[24] Kuznetsov, A.V., Nield, D.A., Natural convective boundary-layer flow of a nanofluid past a vertical plate, *International Journal of Thermal Sciences*, 49, 2010, 243-247.

[25] Sheikholeslami, M., Hayat, T., Alsaedi, A., MHD free convection of Al_2O_3–water nanofluid considering thermal radiation: A numerical study, *International Journal of Heat and Mass Transfer*, 96, 2016, 513-524.

[26] Abdul Hakeem, A.K., Vishnu Ganesh, N., Ganga, B., Magnetic field effect on second order slip flow of nanofluid over a stretching/shrinking sheet with thermal radiation effect, *Journal of Magnetism and Magnetic Materials*, 381, 2015, 243-257.

[27] Ogulu, A., Makinde, O. D., Unsteady hydromagnetic free convection flow of a dissipative and radiating fluid past a vertical plate with constant heat flux, *Chemical Engineering Communications*, 196, 2009, 454-462.

[28] Armaghani, T., Kasaeipoor, A., Alavi, N., Rashidi, M.M., Numerical investigation of water-alumina nanofluid natural convection heat transfer and entropy generation in a baffled L-shaped cavity, *Journal of Molecular Liquids*, 223, 2016, 243-251.
[29] Makinde, O.D., Aziz, A., Boundary layer flow of a nanofluid past a stretching sheet with a convective boundary condition, *International Journal of Thermal Sciences*, 50, 2011, 1326-1332.
[30] Sajjadi, H., Amiri Delouei, A., Izadi, M., Mohebbi, R., Investigation of MHD Natural Convection in a Porous Media by Double MRT Lattice Boltzmann Method utilizing MWCNT–Fe3O4/Water Hybrid Nanofluid, *International Journal of Heat and Mass Transfer*, 132, 2019, 1087-1104.
[31] Alsabery, A.I., Mohebbi, R., Chamkha, A. J., Hashim, I., Effect of local thermal non-equilibrium model on natural convection in a nanofluid-filled wavy-walled porous cavity containing inner solid cylinder, *Chemical Engineering Science*, 201, 247-263, 2019.
[32] Izadi, M., Mohebbi, R., Amiri Delouei, A., Sajjadi, H., Natural convection of a Magnetizable hybrid nanofluid inside a porous enclosure subjected to two variable magnetic fields, *International Journal of Mechanical Sciences*, 151, 2019, 154-169.
[33] Sheikholeslami, M., Rashidi, M.M., Effect of space dependent magnetic field on free convection of Fe_3O_4-water nanofluid, *Journal of the Taiwan Institute of Chemical Engineers,* 56, 2015, 6-15.
[34] Garoosi, F., Bagheri, G., Rashidi, M.M., Two phase simulation of natural convection and mixed convection of the nanofluid in a square cavity, *Powder Technology*, 275, 2015, 239-256.
[35] Hady, F.M., Eid, M.R., Abd-Elsalam, M.R., Ahmed, M.A., Soret effect on natural convection boundary-layer flow of a non-Newtonian nanofluid over a vertical cone embedded in a porous medium, *IOSR Journal of Mathematics*, 8(4), 2013, 51-61.
[36] Arafune, K., Hirata, A., Interactive solutal and thermal Marangoni convection in a rectangular open boat, *Numerical Heat Transfer, Part A: Applications: An International Journal of Computation and Methodology,* 34(4), 1998, 421-429.
[37] Savino, R., Monti, R., Oscillatory Marangoni convection in cylindrical liquid bridges, *Physics of Fluids*, 8(11), 1996, 2906-2921.
[38] Sastry, D.R.V.S.R.K., Murti, A.S.N., Poorna Kantha, T., The effect of heat transfer on MHD Marangoni boundary layer flow past a flat plate in nanofluid, *International Journal of Engineering Mathematics*, 581507, 2013, 6 pages.
[39] Chen, Y., David, S.A., Zacharia, T., Cremers, C.J., Marangoni convection with two free surfaces, *Numerical Heat Transfer, Part A: Applications*, 33(6), 1998, 599-620.
[40] Golia, C., Viviani, A., Cioffi, M., Thermocapillary bubble migration in Confined Medium, *Actn Astronaurica*, 38(3), 1996, 193-208.
[41] Christopher, D.M., Wang, B., Prandtl number effects for Marangoni convection over a flat surface, *International Journal of Thermal Sciences*, 40, 2001, 564-570.
[42] Aly, E.H., Ebaid, A., Exact analysis for the effect of heat transfer on MHD and radiation Marangoni boundary layer nanofluid flow past a surface embedded in a porous medium, *Journal of Molecular Liquids*, 215, 2016, 625-639.
[43] Arifin, N.M., Nazar, R., Pop, I., Marangoni driven boundary layer flow past a flat plate in nanofluid with suction/injection, *AIP Conference Proceedings,* 1309, 2010, 94-99.
[44] Arifin, N.M., Nazar, R., Pop, I., Marangoni-driven boundary layer flow in nanofluids, *Proceedings of the 2010 international conference on theoretical and applied mechanics 2010 and 2010 International Conference on Fluid mechanics and Heat and Mass Transfer*, 2010, 32–35.
[45] Lin, Y., Zheng, L., Zhang, X., Radiation effects on Marangoni convection flow and heat transfer in pseudo-plastic non-Newtonian nanofluids with variable thermal conductivity, *International Journal of Heat and Mass Transfer*, 77, 2014, 708–716.
[46] Hamid, R.A., Arifin, N.M., The effect of wall suction/injection on MHD Marangoni convection boundary layer flow in nanofluid, *Proceedings of 21st National Symposium on Mathematical Sciences (SKSM21) AIP conference proceedings*, 1605, 2014, 386-391.
[47] Remeli, A., Arifin, N.M., Nazar, R., Ismail, F., Pop, I., Marangoni-driven Boundary Layer Flow in a Nanofluid with Suction and Injection, *World Applied Sciences Journal*, 17, 2012, 21-26.
[48] Hayat, T., Shaheen, U., Alsaedi, A., Asghar, S., Marangoni mixed convection flow with Joule heating and nonlinear radiation, *AIP Advances*, 5, 2015, 077140.
[49]Chamkha, A.J. , Pop, I., Takhar, H.S., Marangoni mixed convection boundary layer flow, *Meccanica*, 41, 2006, 219-232.
[50] Aly, E.H., Vajravelu, K., Exact and numerical solutions of MHD nano boundary layer flows over stretching surfaces in a porous medium, *Applied Mathematics & Computation*, 232, 2014, 191-204.
[51] Aly, E.H., Ebaid, A., Exact analysis for the effect of heat transfer on MHD and radiation Marangoni boundary layer nanofluid flow past a surface embedded in a porous medium, *Journal of Molecular Liquids*, 215, 2016, 625-639.

How to cite this article: Indumathi N., Ganga B., Jayaprakash R., Abdul Hakeem A.K. Heat Transfer of Hybrid-nanofluids Flow Past a Permeable Flat Surface with Different Volume Fractions, J. Appl. Comput. Mech., 8(1), 2022, 21–35. https://doi.org/10.22055/JACM.2019.14842